Graphene nanoribbons with mixed cove-cape-zigzag edge structure

Carbon 175 (2021) 50–59

Contents lists available at ScienceDirect

Carbon

journal homepage: www.elsevier.com/locate/carbon

Research Article

Graphene nanoribbons with mixed cove-cape-zigzag edge structure

Prashant P. Shinde [a], Jia Liu [a, b], Thomas Dienel [a, c], Oliver Gröning [a], Tim Dumslaff [d], Markus Mühlinghaus [d], Akimitsu Narita [e], Klaus Müllen [d, **], Carlo A. Pignedoli [a], Roman Fasel [a, f, ***], Pascal Ruffieux [a], Daniele Passerone [a, *]

[a] Empa, Swiss Federal Laboratories for Materials Science and Technology, Überlandstrasse 129, 8600, Dübendorf, Switzerland
[b] Department of Physics, University of Erlangen-Nürnberg, 91058, Erlangen, Germany
[c] PARADIM, Department of Materials Science and Engineering, Cornell University, Ithaca, NY, USA
[d] Max Planck Institute for Polymer Research, Ackermannweg 10, 55128, Mainz, Germany
[e] Okinawa Institute of Science and Technology Graduate University, 1919-1 Tancha, Onna-son, Kunigami-gun, Okinawa, 904-0495, Japan
[f] Department of Chemistry and Biochemistry, University of Bern, Freiestrasse 3, 3012, Bern, Switzerland

ARTICLE INFO

Article history:
Received 3 November 2020
Received in revised form
22 December 2020
Accepted 23 December 2020
Available online 29 December 2020

Keywords:
Graphene Nanoribbons
Density functional theory
Bottom-up Synthesis
Clar's structure
Edge modification
Electronic structure

ABSTRACT

A recently developed bottom-up synthesis strategy enables the fabrication of graphene nanoribbons with well-defined width and non-trivial edge structures from dedicated molecular precursors. Here we discuss the synthesis and properties of zigzag nanoribbons (ZGNRs) modified with periodic cove-cape-cove units along their edges. Contrary to pristine ZGNRs, which show antiferromagnetic correlation of their edge states, the edge-modified ZGNRs exhibit a finite single particle band gap without localized edge states. We report the on-surface synthesis of such edge-modified ZGNRs and discuss tunneling conductance *dI/dV* spectra and *dI/dV* spatial maps that reveal a noticeable localization of electronic states at the cape units and the opening of a band gap without presence of edge states of magnetic origin. A thorough *ab initio* investigation of the electronic structure identifies the conditions under which antiferromagnetically coupled, edge-localized states reappear in the electronic structure. Further modifications of the ribbon structure are proposed that lead to an enhancement of such features, which could find application in nanoelectronics and spintronics.

1. Introduction

Some of the exceptional intrinsic electronic, mechanical, optical and thermal properties of graphene [1–3], although extremely fascinating, can be seen as a hindrance for direct applications in nanotechnology. A prominent example is the absence of an electronic band gap that prohibits the use of graphene as the active material in a nanotransistor. However, reducing the size of graphene nanostructures to a degree where quantum confinement becomes relevant opens up a range of opportunities. When quasi-one-dimensional sections of graphene, dubbed graphene nanoribbons (GNRs), are considered, novel electronic (opening of the band gap) and magnetic (creation of localized edge states) features [6,7] emerge which are, however, not generally protected with respect to structural imperfections. The latter routinely appear during the top-down fabrication process like chemical etching or electron-beam lithography [4,35]. The use of bottom-up procedures on the other hand, allows to obtain GNRs with virtually no defects down to the atomic level, by starting from appropriately designed and subsequently synthesized molecular precursors, whose polymerization and cyclodehydrogenation are promoted in a unique way by a metallic substrate. This strategy was first successfully demonstrated about 10 years ago [12] and has subsequently allowed for the on-surface synthesis of GNRs with perfect armchair [12–14] or zigzag edges [10]. For the characterization of both their perfect atomic structure and electronic properties scanning tunneling microscopy (STM) and spectroscopy (STS) have emerged as ideal analytic tools. Besides the prototypical armchair GNRs (AGNR) and ZGNRs, the atomistic control provided by on-surface synthesis can also be exploited for producing novel types of nanostructures. In this context, post-growth structural

* Corresponding author.
** Corresponding author.
*** Corresponding author. Empa, Swiss Federal Laboratories for Materials Science and Technology, Überlandstrasse 129, 8600, Dübendorf, Switzerland.
E-mail addresses: muellen@mpip-mainz.mpg.de (K. Müllen), roman.fasel@empa.ch (R. Fasel), daniele.passerone@empa.ch (D. Passerone).

https://doi.org/10.1016/j.carbon.2020.12.069

modifications have the intrinsic drawback that they either create quasi zero-dimensional structures (*i. e.*, isolated defects) or, if repeated along a ribbon section of sizeable length, a certain degree of randomness in the distribution pattern makes the prediction and control of the resulting properties problematic. Instead, if the modifications are implemented at the level of the molecular precursor, then the polymerization and subsequent cyclization/dehydrogenation of the polymer leads by design to a periodic, regular sequence of a "unit-repeated modification" inherited from the precursor molecule. The bottom-up synthesis approach thus appears uniquely well suited to explore new pathways in nanomaterial design and engineering. On the other hand, through a concerted strategy based on the theoretical screening of possible nanostructures, of which only the most promising are then realized experimentally, computational modelling ranging from simple tight binding through density functional theory (DFT) [8,9,11] to higher-level quasi-particle GW approximation [38,39] have been shown to be very well suited to predict the influence of such atom-level design on electronic and magnetic properties of GNR. Thereby a very efficient experimental and simulation 'toolbox' for the synthesis and the prediction and characterization of the physical properties of GNR is available today. Whereas this toolbox has been widely used to investigate the electronic and magnetic properties of edge-modified ZGNRs, there are hardly any reports on their experimental synthesis and in-depth characterization.

In this work we specifically focus on edge modifications that suppress the antiferromagnetically coupled edge states of ZGNRs [10]. We identify the creation of a "cove-cape-cove" unit at either edge of a ZGNR (Fig. 1a), conceptually obtained by removal of two edge carbon atoms separated by one zag unit, as a fundamental structural modification that creates a "dispersive channel" between two edge sections. The corresponding formation of a band gap is predicted by theory, and finds immediate experimental confirmation.

The first part of the paper describes the on-surface synthesis of a cove-cape-modified ZGNR, using a specifically synthesized molecular precursor, and its structural and electronic characterization with STM, STS and non-contact atomic force microscopy (nc-AFM).

After experimental characterization, we provide a theoretical investigation of the structural family of GNRs with this novel edge modification. In particular, we provide a conceptual rationale for the systematic variations of electronic properties in this family of structures and their implications for the occurrence and quenching of magnetic correlations. The systematic relation we establish for the quenching and reemergence of magnetic correlations in this system can be the basis for understanding the behavior of other edge-modified ZGNRs, since the basic mechanism should not be limited to this specific family of structures.

We thus investigate possible ways to maintain the cape-cove structure and at the same time "reactivate" the localized edge states by blocking the dispersive channel coupling the two edges electronically. In this respect, one possibility is the extension of the zigzag segment of the ribbon edge. Another one, being less obvious, consists of the interruption of the path along which the dispersive bands propagate close to the ribbon edges. By cutting *C*—C bonds along this path, the zigzag regions become isolated, thus resembling the short zigzag termini of the AGNR of width $N = 7$ (7-AGNR) studied previously by Talirz et al. [18]. The emergence of radical centers at the edges and thus of localized states is then discussed in terms of Clar's theory of the aromatic sextet. The paper concludes with a short discussion about the robustness of the electronic structure on the cape-cove arrangement at the edges.

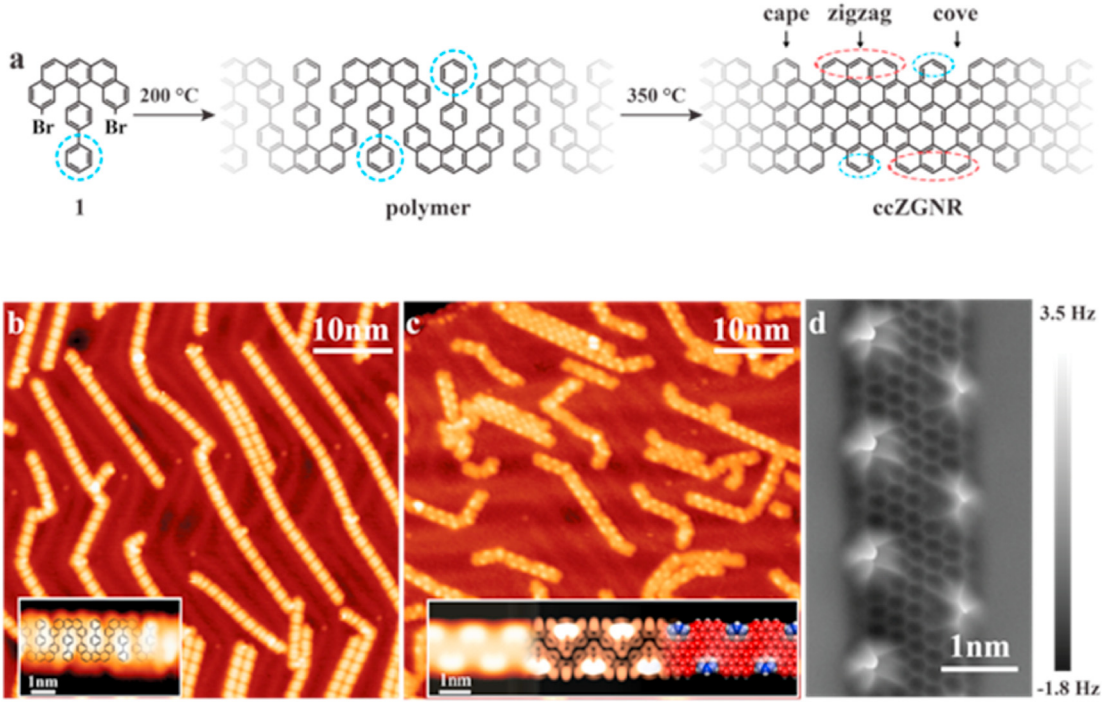

Fig. 1. Mixed cove-cape-zigzag edged graphene nanoribbons (ccZGNRs). (a) Bottom-up synthesis from precursor monomer **1** to polymer and, finally, to the targeted ccZGNR. The phenyl ring which is responsible for bright protrusions in STM images is shown in the blue dashed circle. The zigzag edge that appears darker in the STM and nc-AFM images is highlighted by a red dashed ellipse (b) STM image showing polymer chain formation at 200 °C (V = −1 V, I = 10 pA). (c) STM image after cyclodehydrogenation at 350 °C, showing ccZGNRs (V = −1 V, I = 2 pA). The inset shows a higher-resolution STM image taken at V = −0.8 V, I = 10 pA together with a DFT based STM simulation and the corresponding structural model. (d) High-resolution constant-height nc-AFM image with high frequency shift at the cape parts. Oscillation amplitude, A_{osc} = 70 p.m. The setpoint was set to V = 50 mV and I = 0.01 nA, then the feedback was disabled and the *z*-offset was 0.05 nm closer to the substrate with the bias voltage at V = 5 mV. (A colour version of this figure can be viewed online.)

2. Results

Experimentally, modification of GNR edges can be achieved by altering the chemical design of the molecular precursor involved in the bottom-up synthesis. Over the last years, GNRs with different kinds of edge structures have been synthesized by our laboratory and many other groups. In the present context, zigzag and cove-type edge are the cases most relevant and their synthesis and electronic properties have been reported elsewhere [10,32]. Here, we describe the strategy to achieve a cove-cape-modified ZGNR (ccZGNR), resulting in a mixed cove-cape and zigzag edge structure that has not been realized for GNR to date.

In order to create the proposed structure *via* on-surface synthesis, we designed and synthesized the molecular precursor **1** which is closely related to the one used for fabricating pristine ZGNRs [10]. The structural difference is that precursor **1** does not possess the two methyl groups present in the previous precursor for the pristine ZGNR, which provide closure of the coves to form the smooth extended zigzag edges. Therefore, the lack of methyl groups in precursor **1** leads to the ccZGNR with a combination of the cove and zigzag edge structures while the phenyl ring of **1** (marked by the cyan circle in Fig. 1a) results in a cape between two coves.

The reaction scheme as well as STM and nc-AFM images that characterize the main steps in the synthesis of ccZGNRs are shown in Fig. 1, starting from molecular precursor **1** (Fig. 1a) on an Au (111) surface. The first step is intermolecular coupling reactions through radical addition when the monomer is thermally activated by annealing at 200 °C. At this temperature, the dehalogenated intermediates (carbon-centered biradicals) diffuse on the surface and couple with other radicals, which results in the formation of long polymer chains. As shown in Fig. 1b, the polymer chains exhibit bright protrusions that appear alternatingly on both sides of the polymer axis. They are attributed to the sterically induced out-of-plane conformation of a phenyl-ring at the tail of each monomer (marked by dotted-circles in Fig. 1a). Further annealing at 350 °C promotes the formation of ccZGNRs as shown in Fig. 1c. We observe that most of the ribbons are isolated and randomly oriented with typical lengths between 4 and 30 nm. A closer inspection of the STM images reveals the presence of an asymmetric arrangement of bright protrusions meandering along the ribbon. As for the polymer, these bright protrusions in the final ccZGNR are due to the upward out-of-plane distortion of the cape benzene ring (marked by the cyan ellipses in Fig. 1a) between two coves. The zigzag part of the ribbon edge (see red ellipses in Fig. 1a) appears slightly darker. Later in the paper it will be clarified whether the observed bright protrusions have a purely topographic origin, or are enhanced by the presence of localized electronic states. From the experimental point of view, the uplift of the cape-edge is nicely confirmed by constant-height nc-AFM using a CO-functionalized tip [36]. Fig. 1d reveals a sizeable increase of the resonance frequency at the cape sites, indicating a strong interaction between tip and ribbon. Our density functional theory (DFT)-based STM simulation of a ccZGNR including the alternating arrangement of coves along the two edges of the ribbon correctly reproduces the STM features revealed by the experimental results (inset in Fig. 1c). As described in the "Methods" section, we first optimized the structure of the ribbon on a slab model with which the ribbon interacts *via* a classical force field. We find that the uplift of the cape edge is promoted by an energy gain of ~0.60 eV per unit cell with respect to a reverse geometry where the zigzag edge is uplifted. This energy gain is entirely due to contributions from van der Waals interactions with the substrate. Subsequently, the resulting optimal geometry was used to perform full electronic structure calculations applying periodic boundary conditions in the gas phase.

We used STS to explore the local electronic structure of ccZGNRs as shown in Fig. 2. Differential conductance (dI/dV) spectra, shown as black, blue, and green curves, were measured on the cape-edge, zigzag-edge, and the bare Au (111) surface, respectively (Fig. 2a). A sharp increase in tunneling conductance is observed at the cape unit between the two coves. Within the energy gap, the spectrum obtained on the zigzag-edge reveals a flat local density of states (LDOS). The energy-resolved constant-height dI/dV maps (Fig. 2b) acquired at the energies indicated in the dI/dV spectra (red arrows in Fig. 2a) can be assigned to the band edges near the Fermi energy E_f. In correspondence of the atoms on the cape, we observe either one or two bright spots. These are an effect of the protrusion of the cape away from the ribbon basal plane. From the dI/dV spectra, we estimate a bandgap of 1.8 ± 0.1 eV for the ccZGNR on Au (111).

To elucidate the experimental results, we simulated the dI/dV maps using DFT as shown in Fig. 2c. Our DFT simulations confirm the trends observed in the experimental spectra of Fig. 2b. At higher positive biases (~1.14 eV), we observe two bright spots in the constant-height dI/dV maps which derive from the electronic states localized on the two atoms around the cape (Fig. 2b5 and 2c5). For low negative bias, we again observe two states localized on the cape atoms (see Fig. 2b3 and 2c3). Upon an increase in negative bias, these two states merge into a more extended state and give rise to a brighter spot in the dI/dV maps as shown in Fig. 2b1-2 and 2c1-2.

In Fig. 2d, we analyze the specific atomic contributions to the density of states and to the band structure of ccZGNR, making distinction between the atoms around the cove, on the cape, and the edge atoms. The corresponding projected density of states (PDOS) is normalized by the number of atoms considered in the projection. This analysis reveals a rather uniform spatial distribution of the electronic states belonging to the frontier bands. Indeed, there is no trace of partially flat bands in the electronic band structure of ccZGNRs (Fig. 2f). For a pristine ZGNR in its ground state, the presence of partially flat bands around E_f signals a high density of states and antiferromagnetic correlation between opposite zigzag edges. Unlike the pristine ZGNRs, ccZGNRs are, accordingly to unrestricted DFT calculations, nonmagnetic in their ground state. The theoretical electronic energy gap of ccZGNR with three zigzags is 1.03 eV. The moderate discrepancy between the DFT value of the gap (computed for a structure in "gas phase") and the experimental value of 1.8 eV can be attributed to the fact that the usual DFT underestimation of the gap is here balanced by a measurement where the gap is reduced by screening effects due to the gold substrate [5,15,16]. We note that the main contribution to the occupied states near E_f derives from an extended state. This is clear from Fig. 2e–2(h): The two highest occupied (blue) and lowest unoccupied (red) Kohn-Sham states at the Γ (Fig. 2e) and X (Fig. 2g) points of the one-dimensional Brillouin zone clearly reveal the extended character of those states. In Fig. 2h, an STS simulation at 1.2 Å above the main carbon atom plane of the ribbon is shown, at three different energies marked by the dashed lines in Fig. 2f.

The contribution of a state localized on the cape atoms lies deeper in energy (close to −1.75 eV in Fig. 2d), but it is the height of the cape atoms above the graphene plane that leads to their pronounced appearance in the STS maps in the region near E_f. We thus conclude that the experimentally observed protrusions at small bias voltages arise mainly due to the structural effect given by the uplift of the capes, and not because of localized states present at these functional groups.

It is well known from literature that ZGNRs exhibit a tight-binding electronic structure with an edge state at zero energy with a very narrow peak in the density of states. When spin-dependent electron-electron correlations are included in the treatment, the Stoner criterion is satisfied and the peak splits into

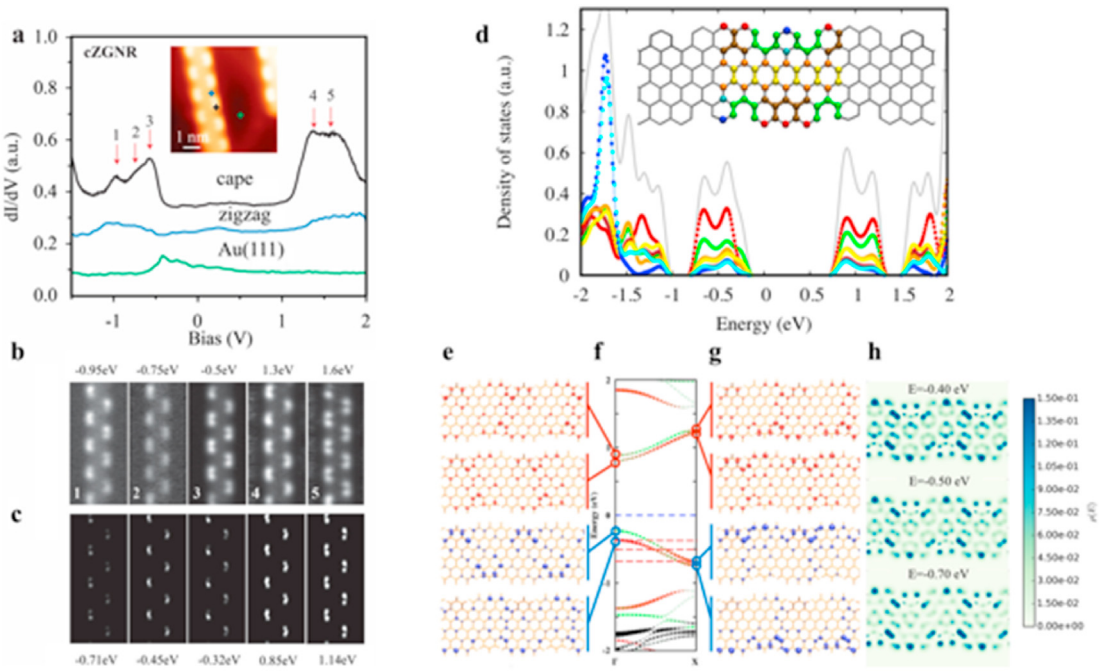

Fig. 2. Electronic structure of ccZGNRs. (a) Differential conductance (*dI/dV*) spectroscopy and experimental (b) as well as DFT-computed (c) LDOS maps. In (a), the location of *dI/dV* spectra is marked in the STM topography in the inset. Black, blue, and green curves are measured on cape, zigzag-edge, and the Au (111) surface, respectively. The red arrows indicate the bias voltages at which the *dI/dV* maps shown in (b) were acquired. The setpoint was V = -1 V and I = 0.01 nA on Au, V = -1 V and I = 0.04 nA on the cape, and V = -1 V and I = 0.04 nA on the zigzag-edge. (b) Experimental constant-height *dI/dV* maps. The setpoint was V = −1 V and I = 0.01 nA, then feedback was disabled and the *z*-offset was closer to the substrate of 0.46 nm for −0.95 V, 0.52 nm for −0.75 V, 0.55 nm for −0.5 V, 0.99 nm for 1.3 V and 1.05 nm for 1.6 V, respectively. (c) Local density of states (LDOS) maps at around 1.5 Å beyond the top of the ccZGNR calculated within DFT. (d) Projected density of states (PDOS) for ccZGNR obtained by using a Gaussian broadening of 0.1 eV, and (e) atomistic model with different regions highlighted by colors, that allow to appreciate the absence of decay of the states from the edge to the ribbon bulk. The Fermi energy is set to 0 eV. Colors in the PDOS (d) refer to the corresponding atoms in the inset. (f) Band structure calculated at the DFT-PBE level (bandgap = 1.03 eV); for each k-point the color and the size represent the character and the intensity of the projection of the wave function on selected atoms as indicated in the caption. The red, green, and black dots correspond to the projection amplitude of the π orbitals of the atom on the zigzag edge, around the cove, and on the cape, respectively. Larger dots indicate a larger projection amplitude. The two highest occupied (blue) and unoccupied (red) Kohn-Sham states at the Γ (e) and X (g) points of the one-dimensional Brillouin zone are plotted, showing the extended character of those states. In (h), an STS simulation at 1.2 Å above the main carbon atom plane of the ribbon is shown, at three different energies marked by the dashed lines in (f). (A colour version of this figure can be viewed online.)

two frontier states that are antiferromagnetically coupled across and ferromagnetically along the edges [30]. We now consider a model to relate the electronic structure of the pristine 6-ZGNR (a zigzag ribbon of width 6 as defined by the customary convention, see Ref. [31]) to the ccZGNR. For this purpose, we group the edge atoms in different regions and mark them in red, black and green (see Fig. 3a). All edge atoms are saturated by a single hydrogen. This single-hydrogen saturation is compatible with our previous computational studies by which we could assess that experimental STM and AFM images are compatible with this termination at zigzag edges [10,18].

Then, we gradually remove the green carbon atoms from the ribbon's edge and examine the impact on the electronic structure, by computing the electronic properties at DFT and tight-binding levels of theory (see methods section). In DFT calculations we gradually detach the "green" CH groups at the ribbon's edge, whereas in tight binding (SI) we reduce the corresponding hopping parameters.

A situation very close to the pristine ZGNR (Δy = 10 p.m., slight stretching of two *C*—C bonds) is shown in Fig. 3b. Projections on edge atoms of different colors are marked with circles of radius proportional to the projection amplitude. Band structure and density of states clearly show the signature of the edge localized bands. In Fig. 3c) and d) we observe the development of dispersive bands upon increasing the distance between the green C atom and the edge (Δy = 130 p.m. and 350 p.m., respectively). The bands with sizeable projection on the green atoms are removed from the band structure diagram for clarity. In Fig. 3e) the band structure and PDOS of the ribbon with the green atoms completely removed is shown, both in the planar and in the experimental geometry with the cape unit lifted, with the resulting under-coordinated C atoms (neighbors to the green carbon atoms, now removed) are passivated by hydrogens. It is seen that the lifting of the cape does not affect the band structure significantly.

Such DFT calculations help us to identify the transformation from ZGNR with magnetic edge states to the trivially "gapped" ccZGNR system. We note that the development of a cove-cape-cove feature strongly affects the electronic structure both qualitatively and quantitatively. Reducing the coupling between specific C atoms at the edge leads to the development of a delocalized electronic band. In the SI we clarify this concept as well as the effect of hybridization between the two sublattices, presenting a simple tight-binding description. It is shown that the A-B sublattice hybridization can be well observed and is connected to the development of a delocalized state.

To better understand why and to what extent the exponentially decaying edge states, typical of the pristine ZGNR, are not evident from the band structure of ccZGNRs, we compare the local density of states (LDOS) (see Fig. 4) for two similar systems: the experimentally studied ccZGNR, and a model with 9 zigzag units ($N_z = 9$) rather than 3 ($N_z = 3$ for the ccZGNR) between two cove-cape-cove units along each edge. We show in panels c and d of Fig. 4 the PDOS of the two systems, and in the panels e to h STS simulations at a height of 1.0 Å above the ribbon atoms along the central axis, which

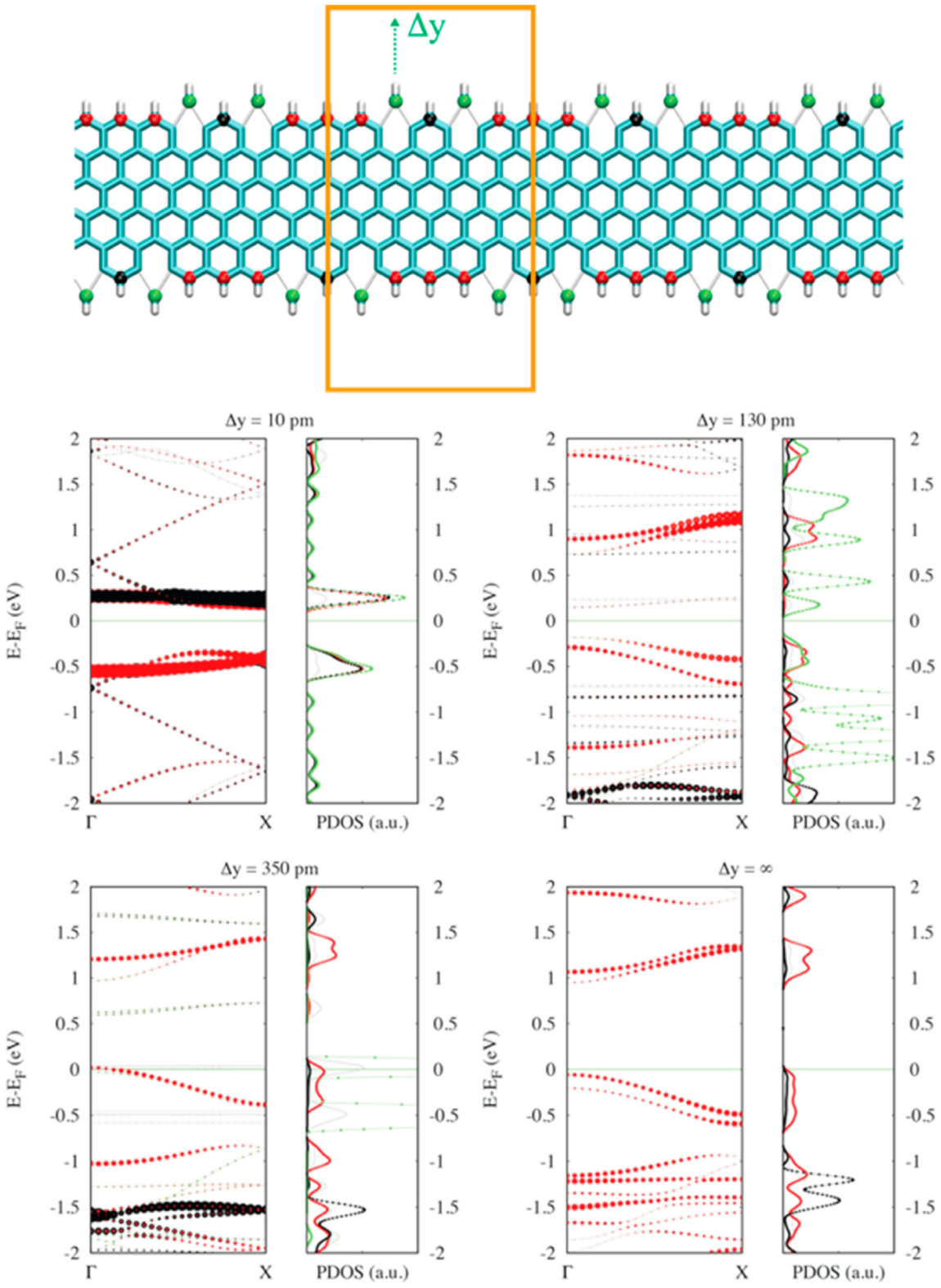

Fig. 3. Gradual modification of a pristine ZGNR into the ccZGNR structure with periodic cove-cape-cove units by removal of selected CH units. (a) Schematic illustration of the ribbon structure, with the gradually removed carbon atom highlighted in green. The unit cell used for the DFT calculations is indicated. (b–d) DFT/PBE band structures with the green C edge atom detached by Δy = 10, 130, 350 and "infinite" pm, respectively. The k-resolved projected density of states (k-PDOS) is shown in (b–e), the contributions from the green atoms are omitted for clarity. They are instead present in the PDOS. Projections on the zigzag edges atoms (red), cape atom (black), the gradually detaching edge C atom (green), and the total PDOS (grey) are shown. Panel e) shows a comparison between the band structures of a ccZGNR in a perfectly flat geometry (blue) and the same ribbon adsorbed on a surface with the experimentally observed non-planar geometry (grey). The emergence of a band gap and the disappearance of edge states corresponds to the developing of dispersive states across the bulk of the structure. (A colour version of this figure can be viewed online.)

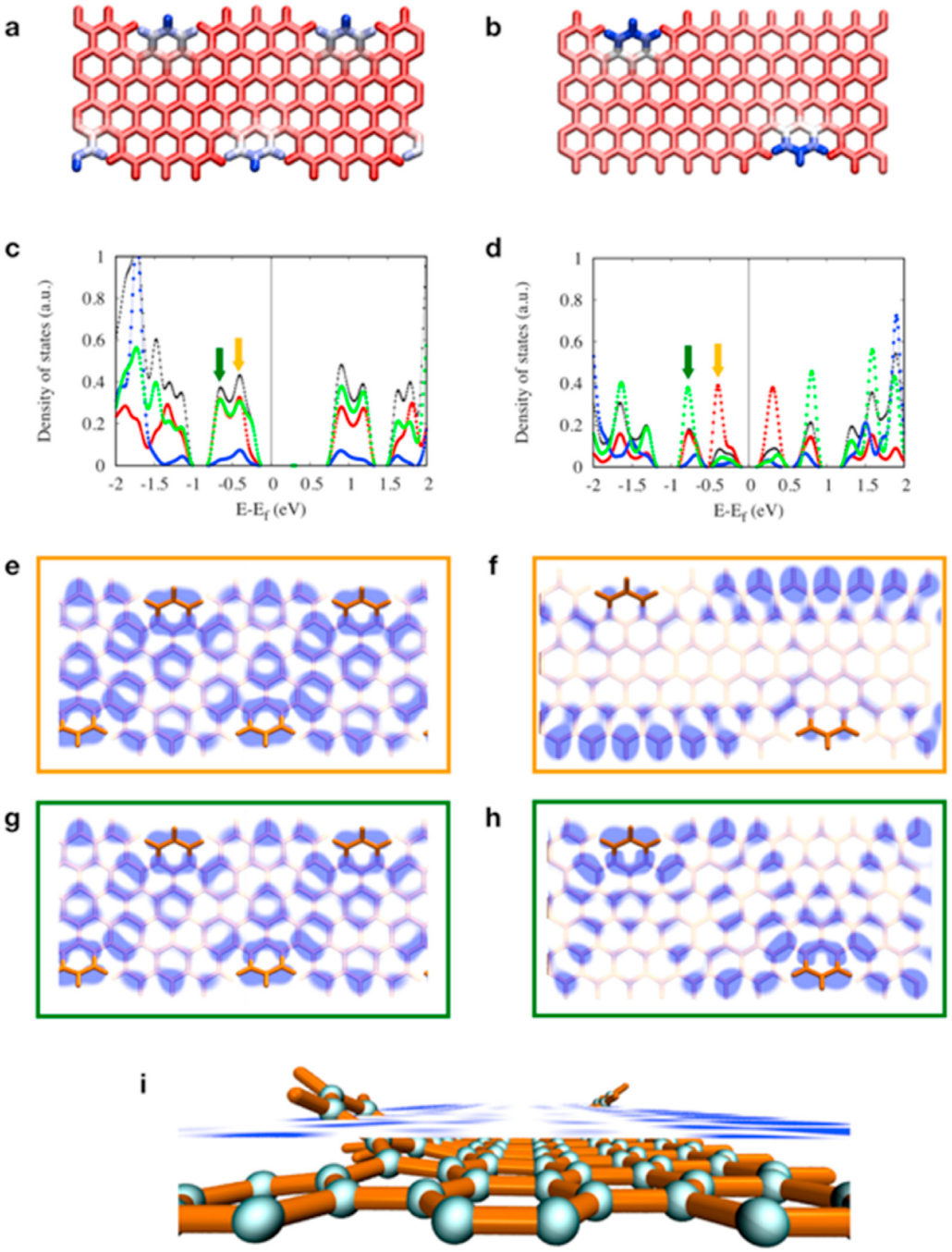

Fig. 4. Impact of zigzag edge segment length on the electronic structure of ccZGNRs. (a,b) Atomistic models of ccZGNR with the number of zigzags between cove defects Nz = 3 (a) and Nz = 9 (b); the colors are coded to the atomic height above the ribbon plane. (c) and (d): Projected density of states (PDOS) for the two cases, projected on atoms around the cove (green), cape top atoms (blue), and zigzag edge atoms (red). (e) to (h): Constant-height STS simulations at a height of 1.0 Å above the ribbon basal plane for the peaks indicated by the corresponding colored arrows in the PDOS (c,d). Note the presence of localized edge states in the Nz = 9 case (orange arrow), whereas the green arrow points to a dispersive band. The orange and green arrows in the Nz = 3 case both point to the dispersive band at slightly different energies. In both systems, states localized at the cape top are located well away from the Fermi energy region. (i): Perspective view of the GNR structure to indicate the level at which the constant-height STS simulations have been performed. (A colour version of this figure can be viewed online.)

reveal the LDOS on a plane cutting the lifted cape units (see Fig. 4i).

For the $N_z = 9$ case, the localized states at the zigzag edges show a LDOS pattern which is well distinguishable from the bulk region of the ribbon (Fig. 4f, states indicated by the orange arrow in the PDOS of Fig. 4d). Conversely, for the other states the signal at the zigzag edges has a similar intensity than in the bulk of the ribbon (Fig. 4e, g, h). Moreover, the main intensity (height) peak showing localization on the cape atoms is located at −1.75 eV with respect to the Fermi energy (red line in the PDOS in Fig. 4c) and similarly at deep energies for the Nz = 9 case (Fig. 4d).

It is thus interesting to understand the stability of spin polarization in ccZGNRs as a function of cove-cape-cove modification concentration or the number of zigzag units (N_z) present between the units (length of pristine zigzag edge segments). Our main concern is the presence of edge localized states as a function of N_z, namely the onset of antiferromagnetism as N_z is increased.

Therefore, we performed first-principles calculations to study the electronic and magnetic properties of ccZGNRs with varying N_z. In experiments, the $N_z = 3$ case, edge states are absent. Our calculations show that spin polarization is completely suppressed for $N_z < 6$, *i. e.*, in presence of a very high concentration of cove-cape-cove edge modifications. Thus, the stability of spin states and the magnetic moments on the zigzag edge C atoms decrease with the concentration accessible in real samples. In addition, spin suppression closely correlates with the reduction and/or removal of the edge states near E_f (see Fig. 5, left panel). For $N_z \geq 6$, the spins are preserved and the systems become magnetic with antiferromagnetic coupling between opposite edges.

Fig. 5 shows effective band structures (unit cell representation) for ccZGNRs with $N_z = 3$ (panel a), 6 (panel b), 9 (panel c) and 15 (panel d). The effective band-structure method (EBS) uses a band unfolding technique to restore the *E(k)* picture in the primitive cell (*pc*). At its core, the EBS method facilitates the determination of the spectral weight of a supercell (*SC*) energy eigenvalue *E(K)* by projecting the corresponding eigenstate on all *pc* Bloch states corresponding to the equivalent *k* [17]. The red circles in Fig. 5 represent the projection amplitude (spectral weight) of the SC eigenvalues. It is clear from these plots that with increasing N_z, the system's electronic structure approaches that of pristine ZGNRs, with small changes around E_f. For $N_z = 15$, we see that the edge state features reappear near the Brillouin zone boundary (X-point). Larger N_z leads to the minimization of direct interaction of the edge modifications and to magnetic exchange interaction within the zigzag edge segments. Therefore, the systems with $N_z \geq 6$ become magnetic with antiferromagnetic coupling across the edges. Furthermore, our calculations show that for $N_z < 6$, the edge states are completely removed and replaced by dispersive bands and some localized states around the cape (see the tight binding calculations in the SI), the PDOS of Fig. 2d, and the sinusoidal spectral function between −1 and 0 eV in Fig. 5, panel a), whereas for $N_z \geq 6$, there are frontier states localized on the zigzag-edge regions.

It has been pointed out that the introduction of one unpaired electron every three zigzag cusps allows to maximize the aromatic sextets (the Clar formula) in infinite monohydrogenated zigzag ribbons, allowing the definition of the pure ZGNR edges as "aromatic edges" [37]. The same principle can be applied to the termini of narrow armchair ribbons of finite size (7-AGNR), which consist of three zigzag cusps [18]. In the case of ccZGNRs, the edge geometry resembles the finite size 7-AGNR with three zigzag cusps isolated by the cove defects. However, for the ccZGNR, the maximum number of aromatic sextets (10 per unit cell) can be found without introducing an unpaired electron at the zigzag-edge (Fig. 6a). Conversely, when a radical per edge is introduced, no more than 8 aromatic rings (Fig. 6b) can be obtained. Thus, Clar's theory seems to support absence of unpaired electrons at the edge as the most stable configuration.

A closer analysis of the calculated Kohn-Sham states in the experimentally accessible ccZGNR case (corresponding to the band structure shown in Fig. 2f) reveals that indeed the frontier bands are characterized by states extending all along the path that diagonally joins the two zigzag edge regions (Figs. 4b and Fig. 2e-g**),** with some spin density localized at the bonds joining the cove with the uplifted cape (Fig. 2h).

In order to further isolate the zigzag edge regions from each other we prepared a model (Fig. 6c) where the lower edge is further modified by cutting the two bonds indicated by a star in Fig. 6a. These particular bonds are chosen by observing the spatial distribution of the dispersive band of Fig. 2f, whose spatial distribution at selected K-points is depicted in Fig. 2e,g. In this way, the perfect closed-shell aromatic structure shown in Fig. 6a is not possible anymore. Now the closed-shell structure allows for a maximum of 8 aromatic rings (Fig. 6c) while several resonance structures with two paired radicals (Fig. 6d) with 8 or 9 aromatic rings are possible. So, it should energetically be more favorable than before that the system develops localized edge bands stemming from unpaired electrons on the zigzag edge regions. Indeed, the band structure presented in Fig. 6e shows the appearance of partially flat bands together with antiferromagnetism. The Kohn-Sham states at the X point (where the bands are flat) show rapidly decaying states starting from the zigzag edge regions. Interestingly, the conjugation is interrupted on one side by cutting the indicated bonds in the figure. For this reason, the most convenient resonant radical structures in Fig. 6d are sought among the ones where the radicals are located in the lower part of the ribbon.

It is interesting to put our results in perspective with the existing literature about ZGNRs with exclusively coved edges (called "coved

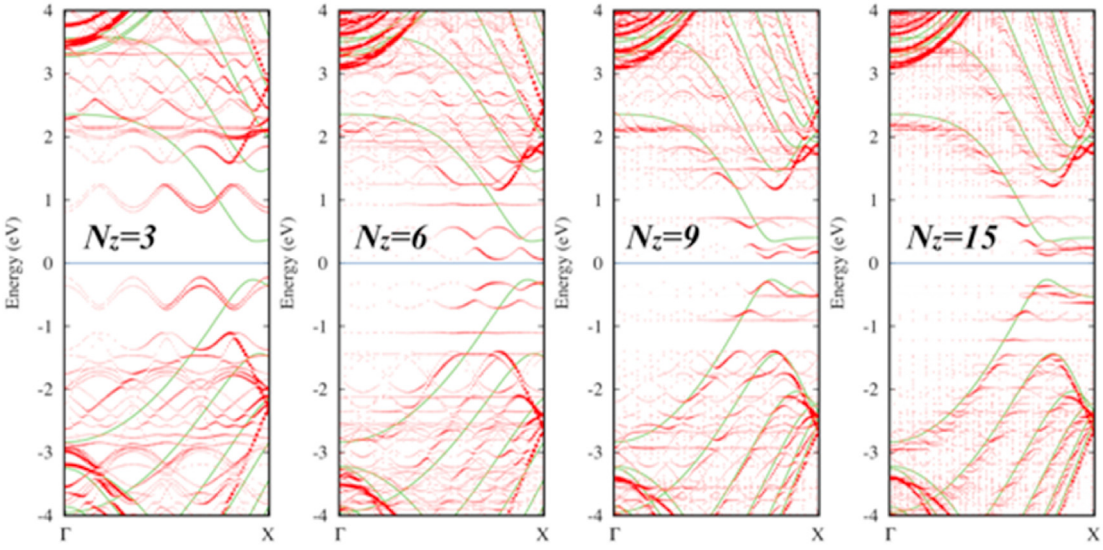

Fig. 5. Effective band structures of ccZGNR structures with increasing distance N_z between the cove-cape-cove units. A primitive cell (*pc*) representation of the band structures of ccZGNRs as a function of N_z simulated using supercells (*SC*). The red dots indicate the amount of Bloch character of the *pc* state preserved in the *SC*. Band structure of the primitive cell is shown by the green lines. The Fermi energy is set to 0 eV. (A colour version of this figure can be viewed online.)

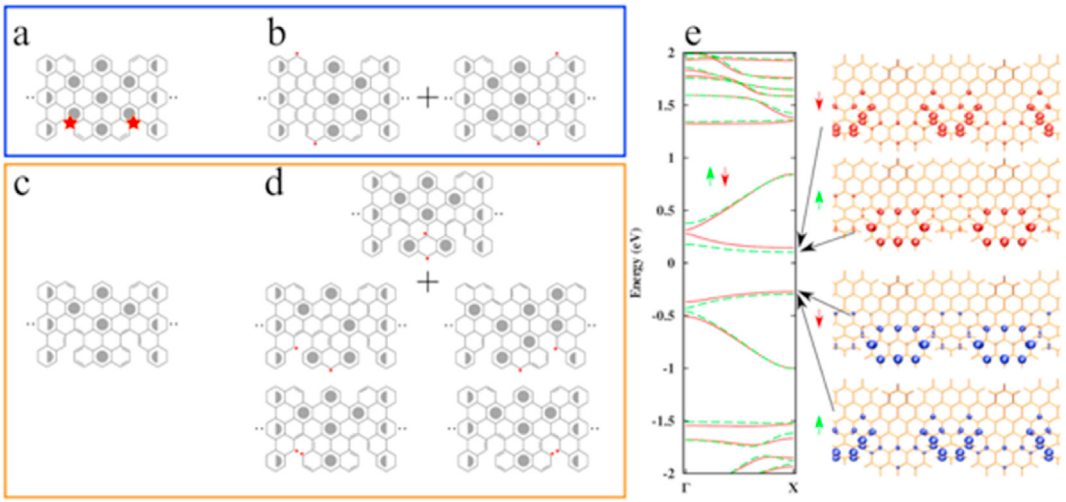

Fig. 6. Aromatic sextet analysis of the ccZGNR. Surrounded by the blue rectangle: Clar structure (maximum aromaticity) for the closed-shell (a) and an example for the biradical (b) configuration of the ccZGNR system. In the biradical case (panel b) the system can accommodate a maximum of 8 aromatic rings with two resonating structures (grey circles); in the closed shell case instead, 10 aromatic rings are possible. Surrounded by the orange rectangle: Clar structure for a modified ccZGNR structure where the bonds marked by stars in panel a) have been cut. In this case, 8 aromatic rings are possible in the closed shell structure (c), and 9 or 8 in the biradical structure (d). Panel e): Band structure and Kohn-Sham states at the X point of the modified ccZGNR model obtained by cutting the bonds marked by stars in panel a). Shown are both the spin-up (green, dashed line) and spin-down (red, continuous line) bands as well as the spin density for the valence-band top and conduction-band bottom that lie at the X point of the supercell Brillouin zone. (A colour version of this figure can be viewed online.)

nanoribbons"), which would correspond to $N_z = 1$ in our nomenclature. It has been shown that graphene with cove edges exhibits partially flat bands, degenerate at the Fermi level, when spin-polarization is not considered. The same result comes from tight-binding calculations of very wide (width N = 30) symmetric-coved ZGNR [32]. Experimentally, coved nanoribbons have been realized [33] with $N = 5$ and the band gap has been measured (on a metallic substrate) at 1.7 eV. The exact geometry of the edges, however, plays an important role in this case [34]. In the supplementary material (Fig. S1) we show that the relative positioning of coves at opposite edges (staggered vs. symmetric) has a dramatic impact on the band structure of the corresponding coved nanoribbon.

3. Conclusion

In conclusion, we have elucidated how the advanced experimental strategy developed in our laboratory allows a controlled modulation of the electronic properties of nanoribbons based on the zigzag edge structure through an appropriate choice of molecular precursors. The different proportion of zigzag, capes, and coves at the ribbon edge leads to magnetic or non-magnetic states, with or without the existence of edge-localized states decaying toward the center of the ribbon. By means of *ab initio* simulations, we were able to derive the corresponding structure-properties relationships. We found that not only the GNR width or the topology of the edges, but also finer structural details interplay in determining the electronic properties of the corresponding GNR. We could realize some models that elucidate the role of the cape/cove modification in suppressing edge states; other models allowed us to determine a critical length of the zigzag edges, above which the similarities to the ZGNR band structure are reflected in a antiferromagnetic ground state. Finally, we showed how the breaking of few *C*—C bonds dramatically affects the aromaticity of the structure, thus restoring the magnetic edge states. All these possible structural modifications may inspire the bottom-up synthesis community toward the design of nanostructures with ever more precisely engineered properties.

4. Methods

All sample preparation and STM and nc-AFM experiments were performed in ultrahigh vacuum systems (ScientaOmicron, base pressure 1×10^{-10} mbar). The Au (111) substrates were cleaned by repeated cycles of Ar^+ sputtering and annealing. Thermal evaporation of the precursor molecules was done by a 6-fold organic evaporator (Mantis GmbH). All measurements were performed at 5 K. The differential conductance *dI/dV* measurements were performed *via* lock-in technique, using a bias voltage modulation of 20 mV at a frequency of 860 Hz *dI/dV* maps were acquired in constant-height mode (feedback off). A commercial tuning fork sensor (ScientaOmicron, resonance frequency 23570 Hz) with attached tungsten tip has been used for nc-AFM. The tip was functionalized by the controlled adsorption of a single CO molecule at the tip apex [19]. The shift in its resonance frequency was recorded in constant-height mode (ScientaOmicron Matrix electronics and HF2Li PLL by Zurich Instruments).

Electronic properties were computed within spin-polarized DFT [20,21] by means of the Quantum-espresso code [22]. We used plane waves as a basis set for the representation of wavefunctions (cutoff 120 Ry) and charge density (cutoff 480 Ry). The atomic cores were described by separable norm-conserving pseudopotentials [23–25] and the PBE approximation for the exchange correlation functional [26]. For Brillouin zone integrations we used a Monkhorst-Pack [27] grid of $12 \times 1 \times 1$ *k*-points. Models used for electronic structure calculations were obtained by relaxing them on a perfect Au (111) slab. The main assumption during geometry optimization was to exclude chemical effects between the molecule and substrate. We describe the molecule within empirical DFT and the substrate *via* embedded atom model (EAM) potentials [28,29]. The interaction between the molecule and substrate was treated through a Lennard-Jones like potential. The vacuum region between replicas in neighboring cells was chosen to be sufficiently large (at least 13 Å) to avoid interactions between neighboring ribbons.

For tight binding calculations, the band structures were calculated with first nearest neighbor tight binding of the C $2p_z$ orbitals

assuming $\gamma_0 = 3$ eV as hopping energy.

In order to clarify the nature of the bands, we plotted the band structure with a color code (white – brown - black) which indicates the weight of the corresponding states on a group of atoms $\mathscr{M}$ for a given band n according to:

$$\alpha_n(k) = \sum_{i \in \mathscr{M}} |i|\psi_n(k)|$$

Here $\alpha_n(k)$ denotes the weight of the nth band at k, $\mathscr{M}$ is the set of considered atomic sites and $|i$ is the C $2p_z$ orbital at site i.

Data availability

All data are available upon request and will be made available on the materials cloud open science data platform (https://www.materialscloud.org/).

CRediT authorship contribution statement

Prashant P. Shinde: Writing - review & editing, Conceptualization, Formal analysis, majority of DFT calculations. **Jia Liu:** Writing - review & editing, On-surface synthesis and microscopy. **Thomas Dienel:** Writing - review & editing, On-surface synthesis and microscopy. **Oliver Gröning:** Writing - review & editing, Supervision, Writing – original draft. **Tim Dumslaff:** Writing - review & editing, Organic synthesis. **Markus Mühlinghaus:** Writing - review & editing, Organic synthesis. **Akimitsu Narita:** Writing - review & editing, Organic synthesis. **Klaus Müllen:** Writing - review & editing, Conceptualization. **Carlo A. Pignedoli:** Writing - review & editing, Software, Supervision, discussion of the results. **Roman Fasel:** Writing - review & editing, Supervision, Writing - original draft. **Pascal Ruffieux:** Writing - review & editing, Supervision. **Daniele Passerone:** Writing - review & editing, Supervision, Writing - original draft, DFT calculations, general paper coordination.

Declaration of competing interest

The authors declare that they have no known competing financial interests or personal relationships that could have appeared to influence the work reported in this paper.

Acknowledgements

We acknowledge illuminating discussions with Shantanu Mishra, the financial support by the NCCR MARVEL (Swiss National Science Foundation), the Swiss National Science Foundation (project 200021_140812) and the Max Planck Society. Calculations were supported by a grant from the Swiss National Supercomputing Center (CSCS) under project ID s746.

Appendix A. Supplementary data

Supplementary data to this article can be found online at https://doi.org/10.1016/j.carbon.2020.12.069.

References

[1] K.S. Novoselov, A.K. Geim, S.V. Morozov, D. Jiang, S.V. Dubonos, I.V. Grigorieva, A.A. Firsov, Electric field effect in atomically thin carbon films, Science 306 (2004) 666.
[2] K.S. Novoselov, A.K. Geim, S.V. Morozov, D. Jiang, M.I. Katsnelson, I.V. Grigorieva, S.V. Dubonos, A.A. Firsov, Two-dimensional gas of massless Dirac fermions in graphene, Nature 438 (2005) 197.
[3] A.K. Geim, Graphene: status and prospects, Science 324 (2009) 1530.
[4] Q.H. Wang, Z. Jin, K.K. Kim, A.J. Hilmer, G.L.C. Paulus, C.-J. Shih, M.-H. Ham, J.D. Sanchez-Yamagishi, K. Watanabe, T. Taniguchi, J. Kong, P. Jarillo-Herrero, M.S. Strano, Understanding and controlling the substrate effect on graphene electron-transfer chemistry via reactivity imprint lithography, Nat. Chem. 4 (2012) 724.
[5] P. Ruffieux, J. Cai, N.C. Plumb, L. Patthey, D. Prezzi, A. Ferretti, E. Molinari, X. Feng, K. Müllen, C.A. Pignedoli, R. Fasel, Electronic structure of atomically precise graphene nanoribbons, ACS Nano 6 (2012) 6930.
[6] F. Schwierz, Graphene transistors, Nat. Nanotechnol. 5 (2010) 487.
[7] Y.-C. Chen, D.G. de Oteyza, Z. Pedramrazi, C. Chen, F.R. Fischer, M.F. Crommie, Tuning the band gap of graphene nanoribbons synthesized from molecular precursors, ACS Nano 7 (2013) 6123.
[8] Y.-W. Son, M.L. Cohen, S.G. Louie, Half-metallic graphene nanoribbons, Nature 444 (2006) 347.
[9] Y.-W. Son, M.L. Cohen, S.G. Louie, Energy gaps in graphene nanoribbons, Phys. Rev. Lett. 97 (2006), 216803.
[10] P. Ruffieux, S. Wang, B. Yang, C. Sánchez-Sánchez, J. Liu, T. Dienel, L. Talirz, P. Shinde, C.A. Pignedoli, D. Passerone, T. Dumslaff, X. Feng, K. Müllen, R. Fasel, On-surface synthesis of graphene nanoribbons with zigzag edge topology, Nature 531 (2016) 489.
[11] Y. Li, W. Zhang, M. Morgenstern, R. Mazzarello, Electronic and magnetic properties of zigzag graphene nanoribbons on the (111) surface of Cu, Ag, and Au, Phys. Rev. Lett. 110 (2013), 216804.
[12] J. Cai, P. Ruffieux, R. Jaafar, M. Bieri, T. Braun, S. Blankenburg, M. Muoth, A.P. Seitsonen, M. Saleh, X. Feng, K. Müllen, R. Fasel, Atomically precise bottom-up fabrication of graphene nanoribbons, Nature 466 (2010) 470.
[13] J. Cai, C.A. Pignedoli, L. Talirz, P. Ruffieux, H. Söde, L. Liang, V. Meunier, R. Berger, R. Li, X. Feng, K. Müllen, R. Fasel, Graphene nanoribbon heterojunctions, Nat. Nanotechnol. 9 (2014) 896.
[14] L. Talirz, P. Ruffieux, R. Fasel, On-surface synthesis of atomically precise graphene nanoribbons, Adv. Mater. 28 (2016) 6222.
[15] Y.J. Zheng, Y.L. Huang, Y. Chen, W. Zhao, G. Eda, C.D. Spataru, W. Zhang, Y.-H. Chang, L.-J. Li, D. Chi, S.Y. Quek, A.T.S. Wee, Heterointerface screening effects between organic monolayers and monolayer transition metal dichalcogenides, ACS Nano 10 (2016) 2476.
[16] N. Kharche, V. Meunier, Width and crystal orientation dependent band gap renormalization in substrate-supported graphene nanoribbons, J. Phys. Chem. Lett. 7 (2016) 1526.
[17] V. Popescu, A. Zunger, Extracting E versus k effective band structure from supercell calculations on alloys and impurities, Phys. Rev. B 85 (2012), 085201.
[18] L. Talirz, H. Söde, J. Cai, P. Ruffieux, S. Blankenburg, R. Jafaar, R. Berger, X. Feng, K. Müllen, D. Passerone, R. Fasel, C.A. Pignedoli, Termini of bottom-up fabricated graphene nanoribbons, J. Am. Chem. Soc. 135 (2013) 2060.
[19] L. Bartels, G. Meyer, K.-H. Rieder, D. Velic, E. Knoesel, A. Hotzel, M. Wolf, G. Ertl, Dynamics of electron-induced manipulation of individual CO molecules on Cu(111), Phys. Rev. Lett. 80 (1998) 2004.
[20] P. Hohenberg, W. Kohn, Inhomogeneous electron gas, Phys. Rev. 136 (1964) B864.
[21] W. Kohn, L.J. Sham, Self-consistent equations including exchange and correlation effects, Phys. Rev. 140 (1965) A1133.
[22] P. Giannozzi, et al., Quantum espresso: a modular and open-source software project for quantum simulations of materials, J. Phys. Condens. Matter 21 (2009), 395502.
[23] Leonard Kleinman, D.M. Bylander, Efficacious form for model pseudopotentials, Phys. Rev. Lett. 48 (1982) 1425.
[24] S. Goedecker, M. Teter, J. Hutter, Separable dual-space Gaussian pseudopotentials, Phys. Rev. B 54 (1996) 1703.
[25] C. Hartwigsen, S. Goedecker, J. Hutter, Relativistic separable dual-space Gaussian pseudopotentials from H to Rn, Phys. Rev. B 58 (1998) 3641.
[26] J.P. Perdew, K. Burke, M. Ernzerhof, Generalized gradient approximation made simple, Phys. Rev. Lett. 77 (1996) 3865.
[27] H.J. Monkhorst, J.D. Pack, Special points for Brillouin-zone integrations, Phys. Rev. B 13 (1976) 5188.
[28] S.M. Foiles, M.I. Baskes, M.S. Daw, Embedded-atom-method functions for the fcc metals Cu, Ag, Au, Ni, Pd, Pt, and their alloys, Phys. Rev. B 33 (1986) 7983.
[29] C.A. Pignedoli, T. Laino, M. Treier, R. Fasel, D. Passerone, A simple approach for describing metal-supported cyclohexaphenylene dehydrogenation: hybrid classical/DFT metadynamics simulation, Eur. Phys. J. B 75 (2010) 65.
[30] O.V. Yazyev, Emergence of magnetism in graphene materials and nanostructures, Rep. Prog. Phys. 73 (5) (2010), 056501.
[31] K. Wakabayashi, K. Sasaki, T. Nakanishi, T. Enoki, Electronic states of graphene nanoribbons and analytical solutions, Sci. Technol. Adv. Mater. 11 (5) (2010), 054504.
[32] K. Wakabayashi, S. Okada, R. Tomita, S. Fujimoto, Y. Natsume, Edge states and flat bands of graphene nanoribbons with edge modification, J. Phys. Soc. Jpn. 79 (2010), 034706.
[33] J. Liu, et al., Toward cove-edged low band gap graphene nanoribbons, J. Am. Chem. Soc. 137 (2015) 6097–6103.
[34] L. Talirz, P. Shinde, D. Passerone, C.A. Pignedoli, Synthesis of Atomically Precise Graphene-Based Nanostructures: A Simulation Point of View, in: A. Gourdon (Ed.), On-Surface Synthesis, Advances in Atom and Single Molecule Machines, Springer International Publishing, 2016, pp. 237–268.
[35] X. Wang, H. Dai, Etching and narrowing of graphene from the edges, Nat. Chem. 2 (8) (2010) 661–665.
[36] L. Gross, F. Mohn, N. Moll, P. Liljeroth, G. Meyer, The chemical structure of a

molecule resolved by atomic force microscopy, Science 325 (5944) (2009) 1110–1114.
[37] T. Wassmann, A.P. Seitsonen, A.M. Saitta, M. Lazzeri, F. Mauri, Structure, stability, edge states, and aromaticity of graphene ribbons, Phys. Rev. Lett. 101 (9) (2008), 096402.
[38] D. Beyer, S. Wang, C.A. Pignedoli, J. Melidonie, B. Yuan, C. Li, J. Wilhelm, P. Ruffieux, R. Berger, K. Müllen, et al., Graphene nanoribbons derived from zigzag edge-encased poly(para-2,9-dibenzo[Bc,Kl]Coronenylene) polymer chains, J. Am. Chem. Soc. 141 (7) (2019) 2843–2846.
[39] J. Wilhelm, D. Golze, L. Talirz, J. Hutter, C.A. Pignedoli, Toward GW calculations on thousands of atoms, J. Phys. Chem. Lett. 9 (2) (2018) 306–312.